ELSEVIER

Biophysical Chemistry 86 (2000) 203–220

Biophysical Chemistry

www.elsevier.nl/locate/bpc

Electroporative fast pore-flickering of the annexin V–lipid surface complex, a novel gating concept for ion transport ☆

Eberhard Neumann*, Peter M. Siemens, Katja Toensing

University of Bielefeld, Faculty of Chemistry, P.O. Box 100 131, D-33501 Bielefeld, Germany

Received 20 January 2000; accepted 3 February 2000

Abstract

In contact with lipid bilayers and Ca^{2+}-ions, the intracellular protein human annexin V (wild-type), $M_r = 35\,800$, forms two types of cation-selective channels for the transport of Ca^{2+}-, K^+-, Na^+- and Mg^{2+}-ions, depending on the protein concentration [AN]. Type (I) channel events are large and predominant at high values $[AN] \geq \overline{K} = 5$ nM at 296 K. At 50 mM Ca^{2+}, symmetrical on both membrane sides, AN added at the *cis* side, the conductance is $g_{Ca}(I) = 22 \pm 2$ pS and at symmetrical 0.1 M K^+-conditions: $g_K(I) = 32 \pm 3$ pS, associated with two mean open-times $\bar{\tau}_1(I) = 0.68 \pm 0.2$ ms and $\bar{\tau}_2(I) = 31 \pm 2$ ms. Monoclonal anti-AN antibodies added to the *trans*-side first increase the mean open-times and then abolish the channel activity, suggesting that type (I) channels refer to a membrane spanning protein complex, probably a trimer T, which at $[AN] > \overline{K}$ changes its membrane organization to a higher oligomer, probably to the side-by-side double-trimer T_2. The smaller type (II) channel events are predominant at low $[AN] \leq \overline{K}$ and refer to the (electroporative) adsorption complex of the monomer. The conductances $g_i(II)$ for symmetrical concentrations depend non-linearly on the voltage $U_m = U_{ext} + U_{AN}$, where $U_{AN} = 0.02 \pm 0.002$ V is the electrostatic contribution of the Ca^{2+}–AN complex and U_{ext} the externally applied voltage. There is only one mean open-time $\bar{\tau}_o(II)$ which is voltage-dependent according to a functional of $b \cdot U_m^2$ where $b = 113.9 \pm 15$ V^{-2}, yielding an activation Gibbs free energy of $G_a = RT \cdot b \cdot U_m^2$. The conformational flicker probability $f_i(II)$ in $g_i(II) = g_i^0(II) \cdot \Gamma_i \cdot f_i(II)$ is non-linearly voltage-dependent according to a functional of $a \cdot U_m^2$. The Nernst term Γ_i refers to asymmetrical ion concentrations. From $a = 50$ V^{-2}, independent of the ion type, we obtain $f_i^0(II) = 0.03 \pm 0.002$ and the

☆ Dedicated to Professor Henryk Eisenberg.

* Corresponding author. Tel.: +49-521-106-2053; fax: +49-521-106 2981.

E-mail address: eberhard.neumann@uni-bielefeld.de (E. Neumann).

PII: S0301-4622(00)00129-0

conductances for the fully open-channel states: $g^0_{Ca}(II) = 69 \pm 3$ pS (0.05 M Ca^{2+}) and $g^0_K(II) = 131 \pm 5$ pS (1.2 M K^+). From the electroporation term $a = \pi\langle r_p^2\rangle\varepsilon_0(\varepsilon_w - \varepsilon_m)/(2\,kTd)$ we determine the mean pore radius of the complex in its fully open state as $\bar{r}_p = 0.86 \pm 0.05$ nm. The adsorbed annexin V (Ca^{2+}) monomer appears to electrostatically facilitate the electric pore formation at the contact interface between the protein and the lipid phase. The complex rapidly flickers and thus limits the ion transport in a voltage-dependent manner.

Keywords: Annexin V-channels; Membrane electroporation; Electroporative flicker-gating; Oligo-channels; Ion-transport theory

1. Introduction

The annexins are a family of calcium-binding proteins presumed to be involved in cell membrane processes such as for instance ion channel formation [1]. Wild-type human annexin V was the first structurally [2,3] and functionally [4–9] characterized ion channel protein with special properties different from conventional ion channel proteins.

The crystal structure of the human annexin V, refined at 2.0 Å resolution [2,3], has revealed a hydrophilic pore of diameter of approximately 0.1 nm in the center of the molecule. The central pore is formed by four helical domains, which are packed pair-wise into two protein modules. The pore is coated with charged residues and filled with a chain of water molecules. Therefore this narrow pore has been proposed to be the conformationally flexible ion conduction pathway [4] of the surface adsorbed annexin V, peripherally bound with its convex surface to the bilayer membrane mediated by calcium ions. The central conductive pore of this adsorption configuration is arranged parallel to the membrane normal. The molecular structures of various crystal forms of annexin V indicate that the internal configuration of each module is highly conserved, yet the orientation of the modules to each other is different in the various forms. Hence there appears to be a conformational variability of the protein. If there is an internal domain mobility of the modules, different ion conduction properties may be related to relative domain flexibilities. Hence the different conductance levels [10] have been attributed to different conformations of the adsorbed channel protein.

The membrane-associative properties of annexin V, revealed for instance by ellipsometric measurements [11], have shown that Ca^{2+}-specific adsorption of the annexin V molecule to the surface of planar phospholipid bilayers induces two-dimensional aggregation of the protein in the membrane surface plane [12]. Chemical crosslinking experiments have identified trimers, hexamers and higher-order oligomers of vesicle-bound annexin V [13]. In the two dimensional (2D) crystals of annexin V bound to lipid monolayers, the characteristic four-domain arrangement of the annexin V monomer has also been confirmed by electron image analysis. The protein molecules bind as trimers with their convex surface which contains the Ca^{2+}-binding sites. A comparison of the 3D reconstruction of annexin V with the high resolution crystal structure shows that the domain structure is preserved in the '2D-crystals' on the lipid monolayer. But the relative orientation of the modules (II/III) and (I/IV) is slightly changed, so that the Ca^{2+}-binding sites in all four domains become flattened and coplanar with the monolayer surface [14,15].

Here, we provide electrical and biochemical data on two types of ion channels which human annexin V (wild-type) and lipid bilayers can form. The type (I) channel events have a larger conductance value and are attributable to membrane-spanning oligomers of annexin V: trimers and probably side-by-side double trimers and higher oligomers of the trimer. On the other hand, the smaller conductance events particularly at low protein concentrations are attributed to the annexin V monomer surface-adsorbed to the bilayer. Further on, we develop the novel concept of fast electroporative flicker gating for ion transport, where the ion motion is limited by a

voltage-dependent conformational flickering and by the externally-induced, yet protein-facilitated electric pore formation in the planar lipid bilayer part of the protein–lipid complex. Since in the absence of annexin V there is no membrane electroporation, the contact interface of the protein–Ca^{2+}–lipid-complex must mediate a facilitation of ion motion through the protein, combined with electroporation of the lipid phase by external electric fields [16].

2. Materials and methods

2.1. Annexin V preparation

Recombinant human annexin V (wild-type) protein, $M_r = 35\,800$, was expressed and purified as previously described [17]. The protein was quantified by the absorbance A_{280} at the wavelength $\lambda = 280$ nm, assuming $A_{280} = 6$ at a concentration of 10 mg/ml^{-1} or 279 μM [18] yielding the absorbance coefficient $\varepsilon_{280} = 21\,508$ M^{-1} cm^{-1} at $T = 293$ K (20°C). Determination of the protein concentration with the bicinchoninic acid (BCA) reagent (Pierce Europe b.v., Holland) according to the manufacture's instructions [19] yielded the same results as the A_{280}-measurements (data not shown).

2.2. Voltage clamp measurements

All chemicals used in the bilayer experiments were of analytical grade. The bilayer chambers contained one of the following buffer solutions (of components in molar concentrations):

Buffer A: 50 mM $CaCl_2$, 10 mM HEPES, pH 7.4 (296 K); Buffer B: 100 mM KCl, 1 mM $CaCl_2$, 10 mM HEPES, pH 7.4 (296 K); Buffer C: 1.2 M KCl, 1 mM $CaCl_2$, 10 mM HEPES, pH 7.4 (296 K); Buffer D: 10 mM KCl, 1 mM $CaCl_2$, 1.375 M sucrose, 10 mM HEPES, pH 7.4 (296 K), isoosmolar to buffer C. The pH value has been adjusted with tetramethylammonium-hydroxide (TMA).

Planar lipid bilayers (diameter ≈ 0.1 mm) were obtained by the monolayer folding technique according to Montal and Mueller [20]. The lipid mixture used is a solution of diphytanoyl-phosphatidylcholine (DPhPC) and phosphatidylserine (PS) 2:1 (w/w) (both lipids from Avanti Polar Lipids Inc., Birmingham, AL, USA), 4 mg ml^{-1} in $CHCl_3$. The monolayers were formed by spreading 5 μl of the lipid solution on the air–water interface and allowing the organic solvent to evaporate [l (liter) = 1 dm^3].

Asymmetric ion concentrations on both sides of the membrane were derived by first preparing the membrane with symmetrical buffer solutions and then exchanging the aqueous solutions in one half cell by the aid of two syringes (5–8 chamber volumes).

The exact ion concentration in the cell was determined by flame emission spectroscopy (FES).

In all current recordings a bilayer clamp BC-525A (Warner Instruments Corporation) was used. The *trans* side of the bilayer chamber was connected to the virtual ground (φ_{trans}). The externally applied voltage U_{ext} is given by

$$U_{\text{ext}} = \varphi'_{cis} - \varphi_{trans} \quad (1)$$

and thus refers to the externally applied potential φ'_{cis} on the *cis*-side, where the annexin V was added (see Fig. 1).

Data were filtered with a self-built four-pole Bessel filter at 100–1000 Hz and stored on a

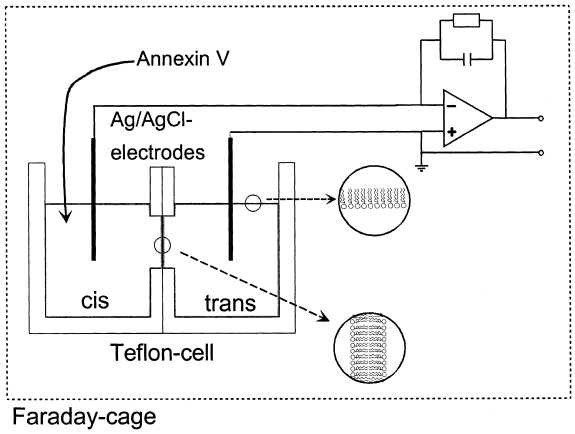

Fig. 1. Schematic representation of the experimental set-up of a planar lipid bilayer, prepared according to the Montal–Müller technique. In all experiments annexin V has been added to the *cis*-side only.

computer (sample rate was five times the filter frequency).

Monoclonal anti-annexin V antibodies were purchased from Kamiya Biomedical Company, Seattle, WA, USA.

3. Results

In Fig. 2a,b, it is seen that annexin V (M_r = 35 800) forms two types of channels (or pores) for the transport of K^+, Na^+, Ca^{2+} and Mg^{2+}-ions across a lipid bilayer membrane. The occurrence of the channel types depends on the protein concentration [AN] and on the membrane voltage U_m.

At high protein concentrations ([AN] > 10^{-9} M), channel events of a larger conductance are dominant (Fig. 2a). The conductance g_i(I) of these type (I) channels is not voltage-dependent, but depends on the type i and the concentration c_i of the ion transported. For instance, in the presence of 50 mM $CaCl_2$ symmetrically on both sides of the membrane, $g_{Ca}(I) = 22$ pS ± 2 pS (Fig. 3). In the presence of 100 mM KCl and 1 mM $CaCl_2$ on both sides of the membrane we obtain $g_K(I) = 32$ pS ± 3 pS. In the presence of 100 mM $MgCl_2$ the conductance is significantly smaller: $g_{Mg}(I) = 14$ pS ± 1.5 pS (data not shown).

At lower protein concentration ([AN] < 10^{-10} M) channel events with a much smaller conductance are detected (Fig. 2b). As seen from the non-linear current–voltage behavior (Fig. 4), the conductance g_i(II) of these type (II) channels is also non-linearly-dependent on the membrane voltage; see below. In the presence of 50 mM Ca^{2+}, g_{Ca}(II) depends unsymmetrically on the sign of the applied external voltage U_{ext}. For example, $g_{Ca}(II) = 3.5$ pS ± 0.4 pS at $U_{ext} = -0.2$ V and $g_{Ca}(II) = 5.85$ pS ± 0.6 pS at $U_{ext} = +0.2$ V in the symmetrical case of 50 Mm $CaCl_2$.

In Fig. 5 it is documented that the type (I) channel activity is dramatically affected by the addition of monoclonal anti-annexin V antibodies (anti-AN-ab) to the *trans* side of the bilayer membrane (where no annexin V was added to the buffer solution). First, approximately 90 s after the addition of the antibodies, the open times are increased up to seconds. Under symmetrical conditions of 0.1 M KCl, the conductance is gradually increasing from $g_K(I) = 32$ pS ± 3 pS to $g_K(I) =$ 48 pS ± 3 pS and finally, approximately 4 min

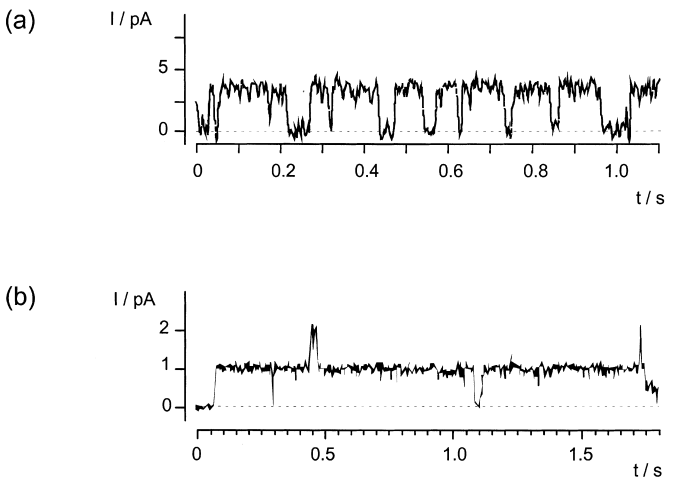

Fig. 2. Channel activities of the complex between annexin V, Ca^{2+} and planar lipid bilayers. (a) type (I) channel and (b) type (II) channel. Externally applied voltage: $U_{ext} = \varphi'_{cis} - \varphi_{trans} = +200$ mV. Buffer: 50 mM $CaCl_2$, 10 mM HEPES (pH 7.4), $T = 296$ K, symmetrical for both membrane sides. Filter frequency: 100 Hz, sample rate: 500 Hz. Lipid composition: diphytanoyl-phosphatidylcholine/phosphatidylserine, DPhPC/PS = 2:1 (w/w). The dashed lines represent the zero current of the closed state of the protein-membrane complex.

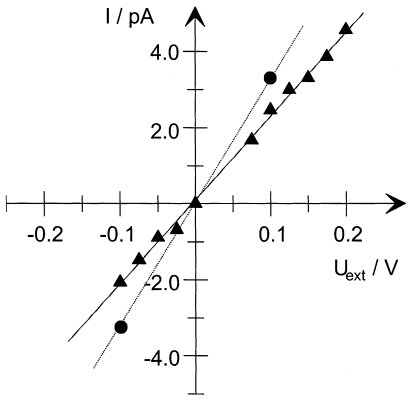

Fig. 3. Current (I/pA) – voltage (U_{ext}/V) behavior of annexin V type (I) channels; ▲, 50 mM $CaCl_2$, 10 mM HEPES (pH 7.4), T = 296 K on both sides of the membrane; ●, in the presence of 100 mM KCl, 1 mM $CaCl_2$, 10 mM Hepes (pH 7.4), T = 296 K on both membrane sides. Filter frequency: 100 Hz, sample rate: 500 Hz.

after addition of antibodies, the channel activity is totally abolished. The data immediately suggest that the channel proteins must be *membrane spanning* such that at least a part of the protein is accessible from the trans side of the membrane. The addition of proteases, as for instance proteinase K to the *trans*-side affects the channel

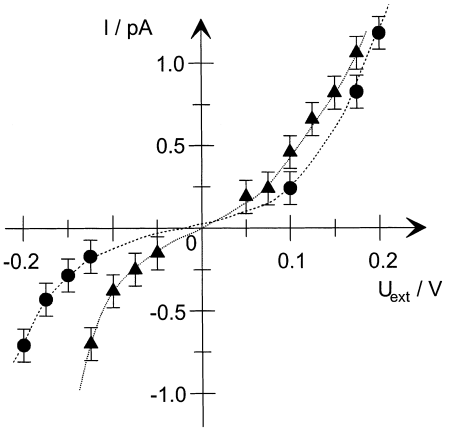

Fig. 4. Non-linear current-voltage behavior of annexin V type (II) channels in the presence of (●), 50 mM $CaCl_2$, 10 mM HEPES (pH 7.4), T = 296 K; (▲), 1.2 M KCl, 1 mM $CaCl_2$, 10 mM Hepes (pH 7.4), T = 296 K. The ionic conditions are symmetrical for both sides. Filter frequency: 100 Hz, sample rate: 500 Hz.

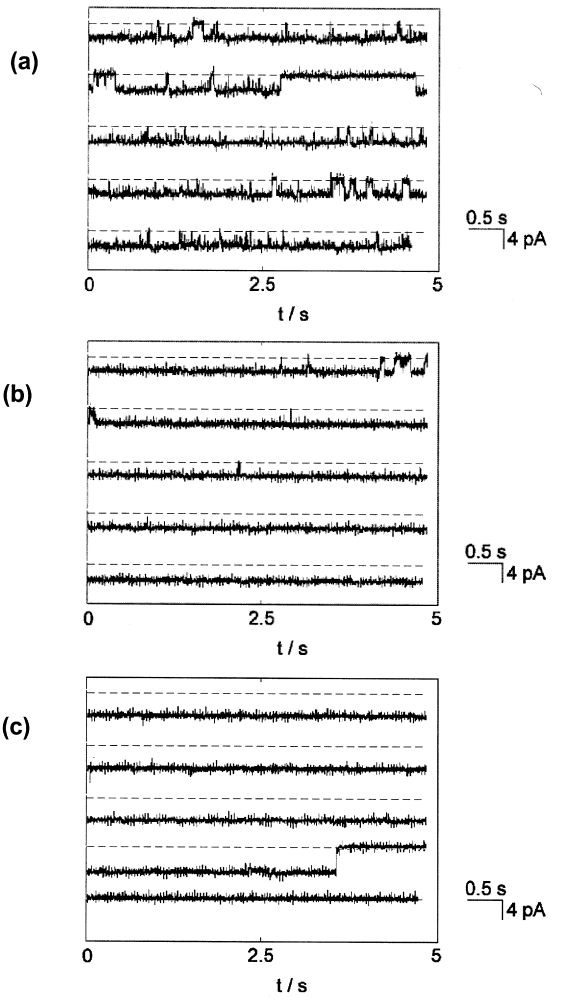

Fig. 5. Anti-annexin V antibody on the *trans* side affects the type (I) channel activity of the AN/Ca^{2+}/bilayer complex. Externally applied voltage: U_{ext} = −100 mV. Symmetrical buffer conditions: 100 mM KCl, 1 mM $CaCl_2$, 10 mM Hepes (pH 7.4), T = 296 K. Filter frequency: 1 kHz, sample rate: 4 kHz. (a) Absence of antibodies (reference traces); (b) type (I) channel activity, at the same conditions as in (a), 90 s after the addition of monoclonal anti-annexin V antibodies to the *trans*-side of the membrane; (c) current fluctuations as in (a) and (b), 4 min after the antibody addition at t = 0. Note that after a long opening period the channel activity ceases and only the zero current of the stable membrane remains; even 30 min later no channel activity reappears. The dashed lines represent the closed state of the annexin V–Ca^{2+}-membrane complex.

activity of the type (I) channels in a very complicated way which is hardly quantifiable. Again, the

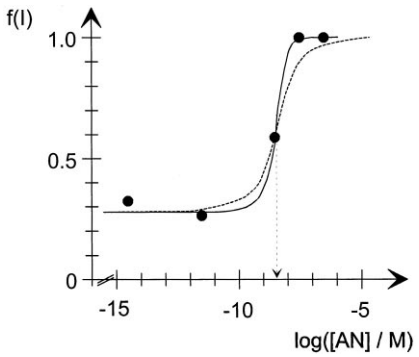

Fig. 6. Concentration dependence of the occurrence of type (I) channel events: f(I), the fraction of experiments resulting dominantly in type (I) channel activity as a function of the annexin V concentration [AN] in the bath solution of the *cis*-side of the planar bilayer. The line represents the level of trimer channel events changing to the level of a side-by-side double trimer, according to Eq. (A8) of the text. The dashed line refers to the Hill-coefficient $h = 1$.

observations as such support the view of a membrane-spanning channel configuration for the type (I) channel.

On the other hand, the type (II) channel (low conductance) is not affected by the addition of anti-annexin V-antibodies, confirming that the surface-adsorbed annexin V on the *cis*-side is the origin of channel(II)-activity in applied voltages.

In Fig. 6 it is seen that the fraction of type (I) channels steeply increases in a narrow concentration range of the annexin V (in the bath solution of the *cis* side) around [AN] ≈ 5 nM, suggesting a cooperative change in the organization of the channel proteins.

The occurrence of two mean open times (Fig. 7), where the contribution (A_1) of the first opening events decreases with the external field, suggests that an overall-open channel state O is coupled with two closed channel states C_1 and C_2.

The rather large overall open-time $\bar{\tau}_o$ of the channel type (II), as seen in Fig. 8, and the non-linear dependence of $\bar{\tau}_o$ on U_m^2 (see Fig. 9), both suggest that these longer open events reflect a kind of voltage-dependent, very fast flicker-gating, associated with the interfacial adsorption complex of the annexin V monomer, Ca^{2+}-ions and the electroporated membrane bilayer.

4. Theory and data analysis

4.1. Type (I)-channel activity

The larger conductance value of lipid bilayer-associated annexin V which preferentially occurs at higher protein concentrations [AN] suggests that oligomers of the annexin V monomer are responsible for the type (I)-channel activity. At $[AN]_{0.5} \approx 5$ nM (Fig. 6) the data indicate a strongly

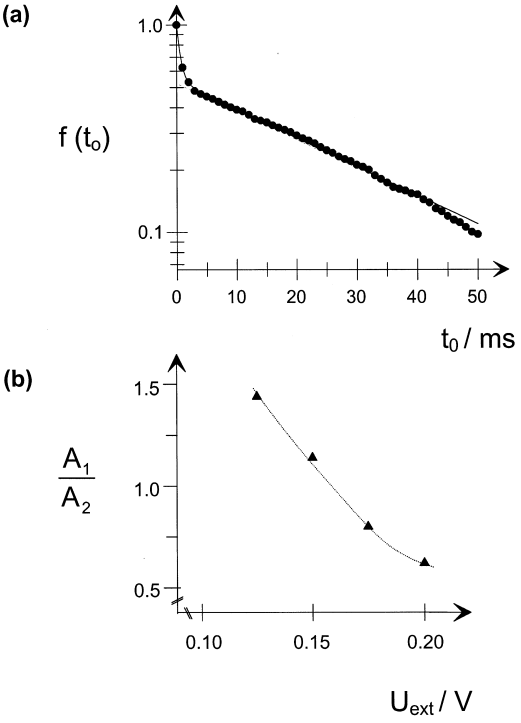

Fig. 7. Example of the mean open time analysis of the annexin V type (I)-channel activity at $U_{ext} = +175$ mV. (a) Fraction $f(t_o)$ of open channels (relative transition probability) as a function of the open time t_o. The continuous line represents the fitting of the experimental data A (●) by the sum of two exponentials, yielding the mean open times $\bar{\tau}_1 = 0.68 \pm 0.2$ ms for the fast phase and $\bar{\tau}_2 = 31 \pm 2$ ms for the slow phase, respectively; (b) the ratio A_1/A_2 of the amplitudes A_1 and A_2 related to the mean open times $\bar{\tau}_1$ and $\bar{\tau}_2$ as a function of external voltage in the range $0.12 \leq U_{ext}/V \leq 0.2$.

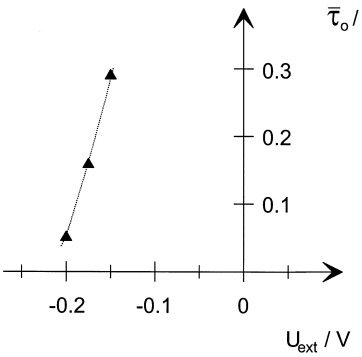

Fig. 8. Mean open time $\bar{\tau}_o$ of annexin V type (II) channels as a function of external voltage in the range $0.2 \geq |U_{ext}/V| \geq 0$. Type (II) channel openings become shorter with increasing voltage, yet they are much larger than those of the type (I) channel.

cooperative change in the organization of the channel complexes, which according to the results of the antibody experiments (see Fig. 5), must be membrane-spanning. It is recalled that annexin V forms trimers (T) and higher oligomers on lipid vesicle surfaces as well as two-dimensional crystals on the surface of lipid monolayers, indicating a tendency for cooperative side-by-side oligomerization of the adsorbed annexins. In any case, the steep increase of the annexin V type (I) channel activity suggests a cooperative transition of trimers to higher oligomers, without a change of the conductance of the single-channel events.

The observation of two mean opening times $\bar{\tau}_1$ and $\bar{\tau}_2$ (Fig. 7) associated with the same type (I) channel activity, which at $U_m \geq |0.1\ V|$ is practically independent of voltage (data not shown), suggests a reaction scheme

$$C_1 \underset{k_{-1}}{\overset{k_1}{\rightleftharpoons}} O \underset{k_2}{\overset{k_{-2}}{\rightleftharpoons}} C_2 \qquad (2)$$

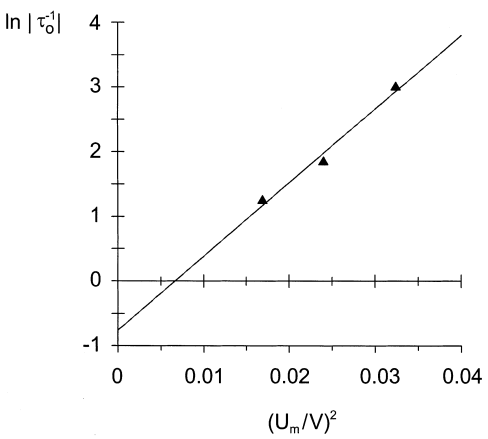

Fig. 9. Membrane voltage dependence of $\bar{\tau}_o/ms$. Graphical representation according to $\ln|\bar{\tau}_o^{-1}|$ vs. U_m^2. Linear regression of the experimental data (▲) according to Eq. (41) yields $\bar{\tau}_o(U_m = 0) = 2.13 \pm 0.25$ s and $b^* = 113.9 \pm 15\ V^{-2}$.

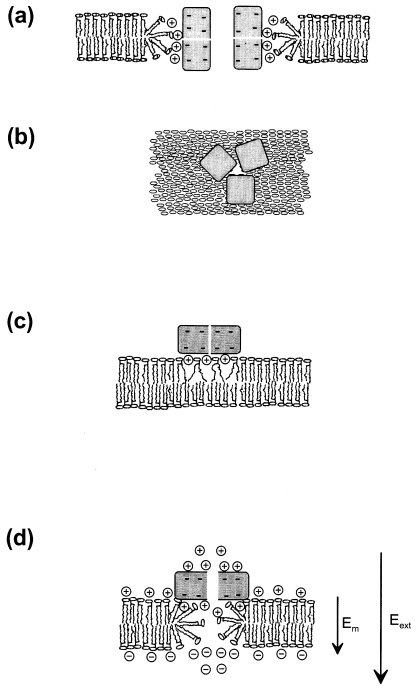

Fig. 10. Schematic representations of the annexin V channel models. (a) Cross-section (side view) of the membrane spanning, trimeric protein–Ca^{2+}-bilayer configuration of the type (I) channel.; ⊕ bound Ca^{2+}-ions of the complex, — anionic protein residues. (b) Top view of type (I)-channel configuration of a trimer. (c) Model for the monomeric AN–Ca^{2+}–lipid surface complex in the non-conductive closed-channel configuration, protein pore diameter ≈ 0.1 nm [8]. (d) Fully-open state of the complex, yielding the type (II) channel activity in the presence of a finite membrane voltage U_m. The ⊕ and ⊖ symbols represent the remaining ions of the externally induced interfacial polarization, causing a hydrophilic membrane pore 'under' the adsorbed annexin V-monomer in the presence of an externally (E_{ext}) induced cross-membrane field E_m. Pore diameter of the complex is ≈ 1.7 nm.

where at least two closed states C_1 and C_2 are coupled to the same open channel configuration O, where $\bar{\tau}_1 = (k_{-1})^{-1}$ and $\bar{\tau}_2 = (k_{-2})^{-1}$. An increase in the membrane voltage appears to shift the reaction sequence in the direction of the closed configuration C_2. Apparently the configuration C_2 has a higher electric moment than state C_1. On the basis of the 3D structure the dipole moment of annexin V has been calculated to be $m = 5 \times 10^{-27}$ C m (1500 debye) [21]. The transition of the adsorbed dipolar protein into a membrane-spanning configuration can then be induced by the electric membrane field ($E_m = U_m/d$ associated with the applied voltage), aligning the protein dipole in the field direction. Three annexin V molecules can provide a larger, electrically symmetric channel configuration as depicted in Fig. 10, accounting for a voltage-independent, larger conductance value. Specifically, bound Ca^{2+}-ions can bridge the edge of a hydrophilic pore [22] with anionic groups of the proteins.

In the simplest case, the highly cooperative change from a low level of occurrence of type (I) channel activity to a high level (Fig. 6) is consistent with a transition of the trimer configuration (T) to a side-by-side double-trimer (T_2) according to the reaction $2T \rightleftharpoons T_2$, being coupled to $3AN \rightleftharpoons T$, as the annexin V concentration increases. The Hill coefficient of this association with respect to the bath concentration [AN] is $h \approx 3$ and $\bar{K}_{AN} = [AN]_{0.5} = 5$ nM (see Appendix A). The oligomerization then increases with the probability of the occurrence of channel (I) events drastically, but must not necessarily change the conductance quality of the events. Of course, oligomerization would increase the occasional superposition of current events. The central pore region of the trimer (as sketched in Fig. 10) contains the glutamate residues 128, 129, 130 and the aspartate residue 137, providing anionic groups as a structural basis for cation selectivity and specificity [23].

4.2. Theory of ion channel transport

4.2.1. The ion-channel structure interaction model

The channel activity data of membrane-associated human annexin V (wild-type) indicate that this protein mediates cation selective transport of Ca^{2+}, K^+, Na^+- and Mg^{2+}-ions.

Classically, the unidirectional flow of ions of type i with charge number z_i (with sign) along the membrane normal is expressed in terms of a flux-density (or flux) vector

$$\phi_i = \frac{1}{A} \cdot \frac{dn_i}{dt} = \frac{c_i \cdot D_i}{RT} \cdot (-\nabla\tilde{\mu}_i) \tag{3}$$

where A is the area of the orifice or mouth of the channel; n_i is the amount, c_i the molar concentration and D_i the diffusion coefficient of ion i *within* the channel volume, respectively. $R = k \cdot N_A$ is the general gas constant, k the Boltzmann constant and N_A the Loschmidt–Avogadro constant, T is the absolute temperature, t the time. The unidirectional flow is driven by the (one-directional) negative gradient ($-\nabla\tilde{\mu}_i$), here $\nabla = d/dx$, of the electrochemical potential

$$\tilde{\mu}_i = \mu_i^{\ominus} + RT \cdot \ln a_i + z_i \cdot F \cdot \varphi \tag{4}$$

where $\mu_i^{\ominus}$ denotes the standard value, $a_i = c_i \cdot y_i/c^{\ominus}$ is the thermodynamic activity, c_i the concentration and y_i the thermodynamic activity coefficient of ion type i, respectively, $c^{\ominus} = 1$ M is the concentration unit, $F = N_A \cdot e_o$ the Faraday constant and e_o the (positive) elementary charge. Note that the electric potential φ at the position of the ion may also contain contributions from surface charges of ionic groups of the membrane components and adsorbed small ions.

Insertion of Eq. (4) in Eq. (3) yields the familiar mole-flux equation of Nernst–Planck for small gradients ($\nabla\tilde{\mu}_i$):

$$\phi_i = -D_i\left[\left(\frac{dc_i}{dx}\right) + \frac{z_i \cdot c_i \cdot F}{RT} \cdot \left(\frac{d\varphi}{dx}\right)\right] \tag{5}$$

Conventionally, for the small concentration gradients the electric potential gradient is approximated by:

$$\frac{d\varphi}{dx} = \frac{\varphi(d) - \varphi(0)}{d} \tag{6}$$

where $\varphi(d)$ and $\varphi(0)$ are the electric potentials at the channel mouths at $x = d$ and $x = 0$, respectively, and d is the channel length.

Consistent with Maxwell's field definition ($E_m = -\nabla\varphi$) the field strength E_m is formally an average quantity given by

$$E_m = -\frac{\Delta\varphi_m}{d} = \frac{U_m}{d} \tag{7}$$

where the membrane potential difference is defined as $\Delta\varphi_m = \Delta\varphi_{trans} - \Delta\varphi_{cis}$.

The frequently encountered saturation in the ion concentration-dependent channel conductance with different saturation and different half-saturation values $(c_i)_{0.5} = K_i$, indicates that there are *transient ion-specific interactions* of the transported ions with the channel structure. The ion-specific interactions are formulated in terms of a degree β_i of transient binding for a specific reaction scheme of *minimum* complexity:

$$i^{cis} + O^{cis} \underset{k_{-1}}{\overset{k_1}{\rightleftharpoons}} (i\cdot O) \underset{k_2}{\overset{k_{-2}}{\rightleftharpoons}} O^{trans} + i^{trans} \tag{8}$$

where the channel orifice O^{cis} of the *cis*-side and that of the *trans*-side O^{trans}, both may individually bind ions i from either side to form a transient complex denoted by $(i\cdot O)$ or $(O\cdot i)$. The k_j with $j = 1, -1, 2, -2$ are the respective rate constants. We may now formally attribute to the configuration $(i\cdot O)$ or $(O\cdot i)$ a concentration c_i^m with the quality of a volume-related probability of finding an ion bound in the channel. This probability is then — in this simple model of one type of site — dependent on the outside concentrations c_i^{cis} *and* c_i^{trans}.

Applying the mass action law of chemical thermodynamics to the binding processes in Eq. (8), we obtain an expression for the degree β_i of transient binding:

$$\beta_i = \frac{c_i^m}{c_i^{\max}} = \frac{c_i}{c_i + K_i^{\ominus}/Y} \tag{9}$$

where $c_i^{\max}$ is the maximum value of c_i^m and the dimensionless quantity $K_i^{\ominus} = K_i\cdot Y/c^{\ominus}$ is the ion-specific thermodynamic equilibrium constant. $K_i = c_i\cdot[O]/[(i\cdot O)]$ is the apparent (concentration-dependent) chemical equilibrium constant. $Y = y_i\cdot y_O/y_{(i\cdot O)}$ is the activity coefficient ratio for the binding process in Eq. (8) and the brackets [ ] denote concentration.

For a $z_+{:}z_-$ interaction between a cation (z_+) and an anionic group (z_-) the Debye–Hückel ion-screening expression for Y reads:

$$\ln Y = -\frac{2A\cdot|z_+\cdot z_-|\cdot\sqrt{I_c}}{1 + B\cdot\sqrt{I_c}}, \tag{10}$$

where A and B are constants, see Atkins [24]. Eq. (10) can be applied to calculate Y for the given molar ionic strength $I_c = 0.5\cdot\sum_i z_i^2 c_i$ of the bath solution.

Returning now to the net ion transport, Eq. (5), the integration of the gradient terms $dc_i(x)/dx$ and $d\varphi(x)/dx$, in the boundaries given already for Eq. (6), yields the general flux equation for the transient site-binding model:

$$\phi_i = \left[\frac{z_i\cdot F\cdot D_i}{RT\cdot d}\cdot c_i^{\max}\cdot\beta_i^{cis}\right]\cdot\frac{e^{b_iU_m} - \beta_i^{trans}/\beta_i^{cis}}{e^{b_iU_m} - 1}\cdot U_m \tag{11}$$

where the definition $b_i = z_iF/RT$ and Eq. (9) for the *cis*-side and the *trans*-side were used, respectively. The validity of using the equilibrium quantity β_i is restricted to higher salt concentrations, such that $k_1\cdot c_i \gg k_{-1}$ and $k_2\cdot c_i^{trans} \gg k_{-2}$. Assuming diffusion controlled approach of the ions to the binding sites, k_1 and k_2 in Scheme 8 are in the order of 10^8–10^{10} M^{-1} s^{-1} [25]. Usually, for monovalent ions, $K_i \geq 0.1$ M and for divalent ions $K_i \geq 10^{-3}$ M. Therefore, $k_{-1} = K_1\cdot k_1$ and $k_{-2} = K_2\cdot k_2$ are in the order of $\geq 10^5$ s^{-1} to $\geq 10^7$ s^{-1}. The unavoidable current recording noise requires higher ion concentrations in the bath solutions, normally $c_i \geq 0.05$–0.1 M. Hence the condition $k_j\cdot c_j > k_{-j}$ can readily be fulfilled.

The complex expression Eq. (11) simplifies for practical limiting cases:

4.2.2. Limiting cases

Symmetrical concentration conditions. If $c_i^{cis} = c_i^{trans} = c_i$ we see that also $\beta_i^{cis} = \beta_i^{trans} = \beta_i$ ap-

plies. The flux for this case is given by

$$\phi_i = \frac{z_i \cdot F \cdot D_i}{RT \cdot d} \cdot c_i^{\max} \cdot \beta_i \cdot U_m \tag{12}$$

where β_i and $c_i^{\max}$ are specified by Eq. (9).

Highly asymmetrical concentration conditions. For the case that $c_i^{cis} \gg c_i^{trans}$, the term β_i^{trans} can be very small compared with β_i^{cis}. Under these conditions

$$\phi_i = \frac{z_i \cdot F \cdot D_i}{RT \cdot d} \cdot c_i^{\max} \cdot \beta_i^{cis} \cdot \Gamma_i \cdot U_m \tag{13}$$

where the notation Γ_i for this limit case here refers to the condition $\beta_i^{trans}/\beta_i^{cis} \ll 1$ such that:

$$\Gamma_i = \frac{e^{b_i U_m}}{e^{b_i U_m} - 1} \tag{14}$$

applies.

4.2.3. Conductances of type (I) channel events

Since the conduction g_i refers to the flow trough an open channel, the fully-open-channel current I^o is given by:

$$I^o = z_i \cdot F \cdot \phi_i = g_i(c_i, U_m) \cdot U_m \tag{15}$$

The condition may be expressed as a product of concentration-dependent factors:

$$g_i(c_i, U_M) = g_i^o \cdot \Gamma_i = g_i^{\max} \cdot \beta_i \cdot \Gamma_i \tag{16}$$

A comparison with Eq. (11) shows that the conductance for symmetrical ion concentration conditions (i.e. $\Gamma_i = 1$) is specified as:

$$g_i^o = \frac{(z_i \cdot F)^2 \cdot D_i}{RT \cdot d} \cdot c_i^{\max} \cdot \beta_i^{cis} \tag{17}$$

The concentration gradient factor is defined by

$$\Gamma_i = \frac{e^{b_i \cdot U_m} - \beta_i^{trans}/\beta_i^{cis}}{e^{b_i \cdot U_m} - 1} \tag{18}$$

It is seen that from the relationship $g_i = g_i^o \cdot \beta_i^{cis}$, one may determine g_i^o and thus the product $D_i \cdot c_i^{\max}$ as well as $K_i^{\ominus}$ from experimental concentration dependences.

It is important to realize that the conductance of non-linear current-voltage dependencies, as encountered for asymmetric concentration conditions and with $U_m = U_{\text{ext}}$, is given by the differential operation

$$g_i = \frac{dI}{dU_m} \tag{19}$$

For the condition $c_i \ll K_i$, it is readily derived that $\beta_i^{trans}/\beta_i^{cis} \approx c_i^{trans}/c_i^{cis}$ and that

$$\Gamma_i \cdot U_m = U_m + U_{\text{Nernst}} \tag{20}$$

The zero-current voltage (Nernst potential) for dilute solutions, where the activity coefficient ratio $Y_i^{cis}/Y_i^{trans} \approx 1$ such $a_i^{cis}/a_i^{trans} \approx c_i^{cis}/c_i^{trans}$, is given by

$$U_{\text{Nernst}} = -(\Delta\varphi_{\text{Nernst}})_{I=0} = \frac{R \cdot T}{z_i \cdot F} \cdot \ln \frac{a_i^{cis}}{a_i^{trans}} \tag{21}$$

If therefore the total voltage $(U_m + U_{\text{Nernst}})$ is considered, then the non-linear I/U_m-dependence of asymmetrical concentrations becomes a linear $I/(U_m + U_{\text{Nernst}})$-relationship and the expression

$$g_i = \frac{I}{U_m + U_{\text{Nernst}}} \tag{22}$$

where here for type (II) channel-activity $U_m = U_{\text{ext}}$ holds.

The type (I) channel data have been evaluated using Eqs. (15)–(18). As expected for symmetrical conditions of equal ion concentration on both membrane sides, the conductance $g_i = g_i^o$ are independent of voltage. The actual g_i-values, however, are also dependent on the lipid composition, in particular on the amount of anionic lipids serving as reaction partners for the Ca^{2+}-bridges to the annexin V anionic groups. For instance, as documented in Fig. 3, $g_{Ca}(I) = 22 \pm 2$ pS for symmetrical conditions of 50 mM $CaCl_2$. At the same Ca^{2+} conditions, but a different lipid composition (phosphatidylserine: phosphatidylethanolamin, 9:1), it has been found that $g_{Ca} = 29.5 \pm 1.6$ pS [8].

4.2.4. Channel-transport efficiency

The transport efficiency of a channel for various ions can be estimated on a relative scale for different bath concentrations c_i. On the basis of Eqs. (9) and (17), we now define an efficiency ratio r, here for the type (I)-channel events of the Ca^{2+}- and the K^+-ion transport, by the expression:

$$r(\mathrm{I}) = \frac{g^o_{\mathrm{Ca}}}{g^o_{\mathrm{K}}} = \frac{z^2_{\mathrm{Ca}} \cdot D_{\mathrm{Ca}} \cdot \beta_{\mathrm{Ca}}}{z_{\mathrm{K}} \cdot D_{\mathrm{K}} \cdot \beta_{\mathrm{K}}} \tag{23}$$

Note that in our model of the permselective, electrodiffusive ion-binding, Scheme (8), the (volume-related) maximum probability of finding an ion transiently bound always refers to (the same unit) one. Therefore, in this model all $c_i^{\max}$ are equal, independent of ion type i. Hence, here $c_{\mathrm{Ca}}^{\max} = c_{\mathrm{K}}^{\max}$ and $r(\mathrm{I})$ is given by Eq. (23)

In previous approaches to quantify ion-transport specificities, the Nernst-distribution law for membrane-internal free ions (c_i^m) expressed by the distribution coefficient $\gamma_i = c_i^m / c_i$ was applied and the permeability coefficient P_i has been defined by [26]

$$P_i = \frac{\gamma_i \cdot D_i}{d}.$$

In this sense, our transport parameter

$$T_i = z_i^2 \cdot D_i \cdot \beta_i \tag{24}$$

cast in the form of $z_i^2 \cdot D_i \cdot \beta_i / d$, has the quality of a modified permeability coefficient for a given concentration c_i.

Applying now Eq. (23) to our experimental quantities $g_{\mathrm{Ca}}(\mathrm{I}) = g^o_{\mathrm{Ca}}(\mathrm{I}) = 22$ pS at $c_{\mathrm{Ca}} = 0.05$ M and $g_{\mathrm{K}}(\mathrm{I}) = g^o_{\mathrm{K}}(\mathrm{I}) = 32$ pS at $c_{\mathrm{K}} = 0.1$ M, where in both cases $\Gamma_{\mathrm{Ca}} = \Gamma_{\mathrm{K}} = 1$, and $z^2_{\mathrm{Ca}} = 4$ and $z^2_{\mathrm{K}} = 1$, we obtain with Eq. (24): $T_{\mathrm{Ca}} = 0.69 \cdot T_{\mathrm{K}}$. This implies that under the given concentration conditions the transport efficiency of the channel system for K^+-ions is by a factor of approximately 1.5 better than for Ca^{2+}-ions.

To be closer to the conventional permeability coefficient ratio $P_{\mathrm{Ca}}/P_{\mathrm{K}} = \gamma_{\mathrm{Ca}} D_{\mathrm{Ca}} / \gamma_{\mathrm{K}} D_{\mathrm{K}}$, we see that the ratio $\beta_{\mathrm{Ca}} D_{\mathrm{Ca}} / \beta_{\mathrm{K}} D_{\mathrm{K}}$ is given by $T_{\mathrm{Ca}}/4T_{\mathrm{K}} = 0.17$. Therefore on this level, the permeation of K^+ is approximately 5 times better than that of Ca^{2+}. Applying Eqs. (23) and (24) to the comparison between Ca^{2+}- and Mg^{2+}-ions, where $g_{\mathrm{Mg}}(\mathrm{I}) = 14$ pS at $c_{\mathrm{Mg}} = 0.1$ M, we obtain $r(\mathrm{I}) = T_{\mathrm{Ca}}/T_{\mathrm{Mg}} = 1.6$. This means that for the specified concentration conditions the Ca^{2+}-transport of the channel is by a factor of 1.6 more efficient than for the Mg^{2+}-transport.

4.3. Type (II) channel activity

Since the type (II)-channel activity is not affected by proteases and anti-annexin V antibodies added to the *trans*-side of the bilayer, the channel activity must be due to the adsorbed annexin V on the *cis*-side. The rather long mean open times $\bar{\tau}_o$ and the voltage dependence of both $\bar{\tau}_o$ and the conductances $g_i(\mathrm{II})$ at symmetrical ion concentration conditions, are suggestive for a fast, but temporarily not-resolvable flickery opening in an overall channel-open period, mediated by the interactive passage of ions in an external electric field through the protein–Ca^{2+}–lipid complex (see Fig. 10).

Voltage-dependent fast flicker-gating has been discussed in the context of channel block by drugs or by the transported ion itself [27]. The theory of conformational flickering between two different open states of a channel protein has been developed by Läuger et al. [10]. Here we develop our model of *electroporative flicker gating*. The novel concept comprises the coupling of the lipid membrane electroporation with conformational (open-closed) flexibility [3] of the adsorbed annexin V. The rapid (not visible) flickering refers to a closed state and a fully open state of the lipid–protein complex during an overall-open period embedded in two overall-closed periods. It is emphasized that the rapid flickering as such cannot be temporarily resolved because of instrumental limitations (approx. 10 kHz). The conformational flicker frequency of the protein–lipid complex thus is larger than 10^4–10^5 Hz.

The conductance $g_i(\mathrm{II})$ associated with the type (II)-current events $\mathrm{I} = g_i(\mathrm{II}) \cdot U_m$ is specified by

$$g_i(\mathrm{II}) = g_i^o(\mathrm{II}) \cdot \Gamma_i(\mathrm{II}) \cdot f_i(\mathrm{II}) \tag{25}$$

where g_i^o(II) is the conductance of the fully open channel of type (II), Γ_i(II) is the concentration gradient factor given by Eq. (18). The fraction f_i(II) to which the fully open state [with g_i^o(II)] contributes to the actually measured conductance g_i(II) is given by the fraction of the open configuration of the protein–lipid complex.

4.3.1. Lipid bilayer membrane electroporation

Membrane electroporation in the absence of adsorbed annexin V is consistently described by a transition between closed lipid bilayer states C and electroporated states (or pores) P according to the scheme [28,29]

$$\mathrm{C} \underset{\mathrm{k}_{-p}}{\overset{\mathrm{k}_p}{\rightleftharpoons}} \mathrm{P} \tag{26}$$

The relaxation rate for this process is given by $1/\tau_p = k_p + k_{-p} = k_{-p}\cdot(1+K)$.

Since $K \ll 1$, the approximation $1/\tau_p = k_{-p}$ holds. Because k_p^{-1} is the mean life time $\bar{\tau}_o$ of the open state P, we see that $\tau_p = \bar{\tau}_o$. For lipid bilayer vesicles τ_p is in the order of 1–5 μs and decreases with the membrane field E_m [30]. In order to account for non-conductive and conductive pores, the scheme C ⇌ P has been specified to C ⇌ HO ⇌ HI, where the hydrophobic pore state HO represents the non-conductive lipid pore and the hydrophilic or inverted pore state HI conducts small ions [30].

4.3.2. Electroporative flicker gating

The mean overall open-time $\bar{\tau}_o$ of the protein–lipid complex is in the order of 2 s (at $U_m = 0$) and decreases with membrane voltage U_m (or field E_m) to $\bar{\tau}_o = 0.05$ s at $|U_m| = 0.2$ V. Even at $U_m = \pm 0.2$ V the pure lipid bilayer does not show conductance events and hence is not conductively electroporated. If there are water-filled, probably non-conductive HO-pores, their lifetime of approximately ≤ 1 μs is not long enough to permit ions to permeate.

In the annexin V–Ca^{2+}–lipid complex, electric pore formation in applied external fields is not only facilitated but also the mean life time $\bar{\tau}_o$ of the lipid–protein pore is enormously increased (Fig. 9). It is recalled that the crystal structure of annexin V aggregates on lipid monolayers is almost identical with that of the 3D crystals, in particular the central pore diameter remains small (0.1 nm). In the fast flickering lipid–protein complex the protein pore in the presence of an external field must have at least transiently a larger diameter, say ≥ 0.6 nm, to permit ion transport of small cations.

If we model the conformational flickering of the complex by the scheme

$$(\mathrm{C}) \underset{k_{-c}}{\overset{k_c}{\rightleftharpoons}} (\mathrm{O}), \tag{27}$$

where the fully open state (O) is associated with the conductance g_i^o(II), for symmetrical ion concentration conditions [i.e. Γ_i(II) = 1]. The fraction of the overall open-time with which the state (O) is actually apparent in the measured conductance $g_i(\mathrm{II}) = g_i^o(\mathrm{II})\cdot f_i(\mathrm{II})$ is given by

$$f_i(\mathrm{II}) = \frac{[\mathrm{O}]}{[\mathrm{O}]+[\mathrm{C}]} = \frac{K}{1+K} \tag{28}$$

In Eq. (28), $K = [\mathrm{O}]/[\mathrm{C}] = f_i(\mathrm{II})/[1 - f_i(\mathrm{II})] = k_c/\mathrm{k}_{-c}$ is the flicker equilibrium constant. Electro-thermodynamically K is expressed as [30,31]:

$$K = K_0 \cdot \mathrm{e}^X \tag{29}$$

The quantity K_0 is the K-value at $E_m = 0$ and the field-effect factor is given by

$$X = \int_0^{E_m} \Delta_r M \,\mathrm{d}E_m/RT \tag{30}$$

In Eq. (30) the term

$$\Delta_r M = N_A \cdot [m(\mathrm{O}) - m(\mathrm{C})] \tag{31}$$

is the reaction dipole moment and m(O) and m(C) are the dipole moments of the open and closed complex configurations, respectively.

In the conventional analysis of membrane electroporation of lipid bilayers, $\Delta_r M = N_A \cdot V_p \cdot \Delta_r P$, where $V_p = \pi \cdot \langle r_p^2 \rangle \cdot d$ is the mean polarized pore volume of the assumed cylindrical electropore of

length d and $\Delta_r P = \varepsilon_0 \cdot (\varepsilon_W - \varepsilon_L) \cdot E_m$ is the chemical reaction polarization, with ε_0 the dielectric permittivity of the vacuum and ε_W and ε_L the dielectric constants of the pore water ($\varepsilon_W \approx 80$) replacing the lipids ($\varepsilon_L \approx 2$) at the pore site.

For this case the exponent X is given by

$$X = \frac{\varepsilon_0 \cdot (\varepsilon_W - \varepsilon_L) \cdot \pi \cdot \langle r_p^2 \rangle \cdot d}{2 \cdot k \cdot T} \cdot E_m^2 = a \cdot U_m^2 \quad (32)$$

where

$$a = \frac{\pi \cdot \langle r_p^2 \rangle \cdot \varepsilon_0 \cdot (\varepsilon_w - \bar{\varepsilon})}{2 \cdot k \cdot T \cdot d} \quad (33)$$

$\bar{\varepsilon}$ being an average value of the components (protein, lipids) which are replaced by water during the formation of an aqueous pore. If $\Delta_r M$ refers to a system of displaceable charged groups, as for instance in a voltage dependent channel protein, we may express $\Delta_r M$ in terms of a polarizability (charge displaceability) tensor α by

$$\Delta_r M = N_A \cdot \alpha \cdot E_m \quad (34)$$

such that the field-effect factor takes the form:

$$X = \frac{\alpha \cdot E_m^2}{2 \cdot k \cdot T} = a \cdot U_m^2 \quad (35)$$

and α is related to the experimental quantity a by

$$\alpha = a \cdot 2 \cdot k \cdot T \cdot d^2 \quad (36)$$

Since usually in the absence of an external field the inequality $K_0 \ll 1$ holds, we have at $E_m = 0$: $f_i^o(\mathrm{II}) = K_0$. Substitution in Eq. (28) specifies the open-probability within a fast-flicker burst event to:

$$f_i(\mathrm{II}) = \frac{f_i^o(\mathrm{II}) \cdot \mathrm{e}^X}{1 + f_i^o(\mathrm{II}) \cdot \mathrm{e}^X} \quad (37)$$

4.3.3. Conductance of type (II)-channels

Insertion of Eq. (37) into Eq. (25) yields the relationship:

$$g_i(\mathrm{II}) = g_i^o(\mathrm{II}) \cdot \Gamma_i \cdot \frac{f_i^o(\mathrm{II}) \cdot \mathrm{e}^X}{1 + f_i^o(\mathrm{II})\, \mathrm{e}^X} \quad (38)$$

Integration of the conductance relationship $d\mathrm{I} = g(\mathrm{II})_i dU_m$ leads to the expression for the single channel current

$$\mathrm{I} = \int_0^{U_m} g_i(\mathrm{II}) \cdot \mathrm{d}U_m = \int_0^{U_m} g_i^o\ (\mathrm{II}) \cdot \Gamma_i \cdot \frac{f_i^o(II) \cdot \mathrm{e}^X}{1 + f_i^o(II) \cdot \mathrm{e}^X} \cdot \mathrm{d}U_m \quad (39)$$

Because this integral can not be solved in a closed form, Eq. (39) must be developed in a Taylor series according to:

$$\mathrm{I} = g_i^o(\mathrm{II}) \cdot \Gamma_i \cdot \left[\frac{f_i^o(\mathrm{II})}{f_i^o(\mathrm{II}) + 1} \cdot U_m + \frac{1}{3} \cdot \frac{a \cdot f_i^o(\mathrm{II})}{(f_i^o(\mathrm{II}) + 1)^2} \cdot U_m^3 - \frac{1}{10} \cdot \frac{a^2 \cdot f_i^o(\mathrm{II}) \cdot (f_i^o(\mathrm{II}) - 1)}{(f_i^o(\mathrm{II}) + 1)^3} \cdot U_m^5 + \ldots \right] \quad (40)$$

Fitting of the experimental data (Fig. 11) with Eq. (40) yields $a = 50 \pm 1\ \mathrm{V}^{-2}$. Applying Eq. (33) and using the estimate $d = 4$ nm (Fig. 12), we obtain the mean pore radius $\bar{r}_p = \langle \bar{r}_p^2 \rangle^{0.5} = 0.86 \pm 0.05$ nm. At $E_m = 0$, the open-probability formally is $f_i^o(\mathrm{II}) = 0.03 \pm 0.002$ and the conductances of the fully open channels formally are $g_{\mathrm{Ca}}^o(\mathrm{II}) = 69\ \mathrm{pS} \pm 3\ \mathrm{pS}$ at 50 mM Ca^{2+} and $g_{\mathrm{K}}^o(\mathrm{II}) = 131\ \mathrm{pS} \pm 5\ \mathrm{pS}$ at 1.2 M K^+, respectively.

The size of the mean pore radius (0.86 nm) is in the same range as that obtained from electro-optic data for lipid vesicles (0.6 nm) [32]

Applying Eq. (36) we find that the polarizability tensor of the complex is $\alpha = 3.45 \times 10^{-38}\ \mathrm{F\ m^2}$. Note that α is equivalent to a volume polarizability of $\alpha_V = (0.7\ \mathrm{nm})^3$, which here is smaller than the pore volume ($d \cdot \pi \cdot r_p^2$).

4.3.4. Interfacially bound Ca^{2+}-ions

The currents of the type (II)-channel events up to $|U_{\mathrm{ext}}| = 0.2$ V are only symmetrical with respect

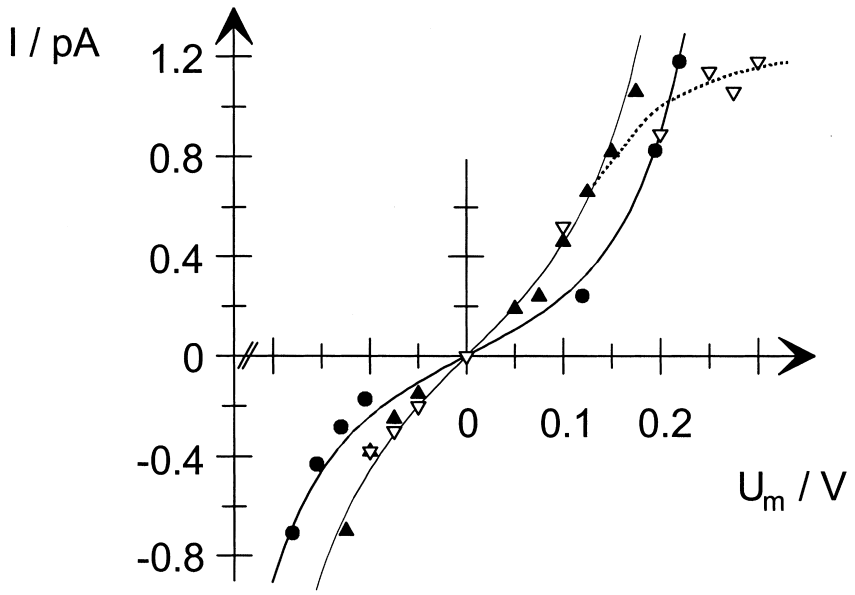

Fig. 11. Analysis of the annexin V type (II) channel current strength–voltage relationship (see Fig. 4) as a function of the calculated effective voltage $U_m = U_{ext} + U_{AN}$, and in the case of asymmetric concentration conditions, $U_m = U_{ext} + U_{AN} + U_{Nernst}$. The solid lines represent the result of the fitting according to Eq. (40) of the text. ●, 50 mM $CaCl_2$ (symmetrical); ▲, 1.2 M KCl (symmetrical) and ▽, unsymmetrical 1.2 M KCl (*cis*)/0.014 M KCl (*trans*). All other conditions are as in Fig. 4.

to positive and negative voltages if we refer to $U_m = U_{ext} + U_{AN} + U_{Nernst}$ (see Figs. 4 and 11). In the case of the example shown here, we have $c_K^{cis} = 1.2$ M KCl, $y_K^{cis} = 0.58$ and $c_K^{trans} = 0.014$ M KCl, $y_K^{trans} = 0.90$. Eq. (21) yields: $U_{Nernst} \approx 0.1$ V.

It is found that for the symmetrical condition of 0.05 M $CaCl_2$, $U_{AN} = 0.02 \pm 0.005$ V. The 'occlusion' of bound Ca^{2+}-ions in the contact plane between the annexin V monomer and the lipid phase (Figs. 10 and 12) establishes an increase $\Delta\varphi_s^{cis} = \varphi_s(AN) - \varphi_s^o$ in the surface potential φ_s relative to the surface potential φ_s^o in the absence of bound Ca^{2+} and annexin V. The bound Ca^{2+}-ions will certainly reduce the absolute value of the negative surface potential φ_s^o arising from the anionic lipid groups (which are a prerequisite for the Ca^{2+}-mediated adsorption of annexin V).

In Fig. 12, $\Delta\varphi_s^{cis} = \Delta\varphi_{AN} = \varphi_{cis} - \varphi'_{cis}$. It is readily seen that, for finite cation currents, $\Delta\varphi_{AN}$ hardly can exceed approximately 0.05 V. Otherwise the electric potential barrier would be too high to permit cation entrance into the protein channel. In addition, the total surface potential at the interfacial plane $\varphi_s^{cis} = \varphi_s^o + \Delta\varphi_{AN} = \sigma_s \cdot \ell / \varepsilon_0 \cdot \varepsilon_W$ is dependent not only on the surface charge density σ_s but also on the Debye–Hückel screening length $\ell = F^{-1} \cdot (\varepsilon_0 \cdot \varepsilon_W \cdot R \cdot T / 2I)^{1/2}$ which itself depends on the ionic strength I_c of the bath solution. At higher ionic strength the value of φ_{cis} and thus that of φ'_{cis} (Fig. 12) is reduced. Of course, on the same line φ_s^{trans} is also ionic strength dependent. The cross-complex potential difference $\Delta\varphi_m = \varphi_{cis} - \varphi_{trans}$ actually then contains the contribution $\Delta\varphi_s$ from asymmetric surface charges and surface charge screening. For the symmetrical concentration conditions $\Delta\varphi_s = \Delta\varphi_{AN}$.

The current for the asymmetrical condition in Fig. 11 begins to saturate at $U_m \approx 0.2$ V. In the presence of a rather high Nernst potential, a further increase in U_{ext} soon meets the transport saturation of the channel for a single-file ion motion.

4.3.5. Gating polarization mechanism

The observed dependence of $\bar{\tau}_o$(II) on the voltage $U_m = U_{ext} + \Delta U_{AN}$ according to

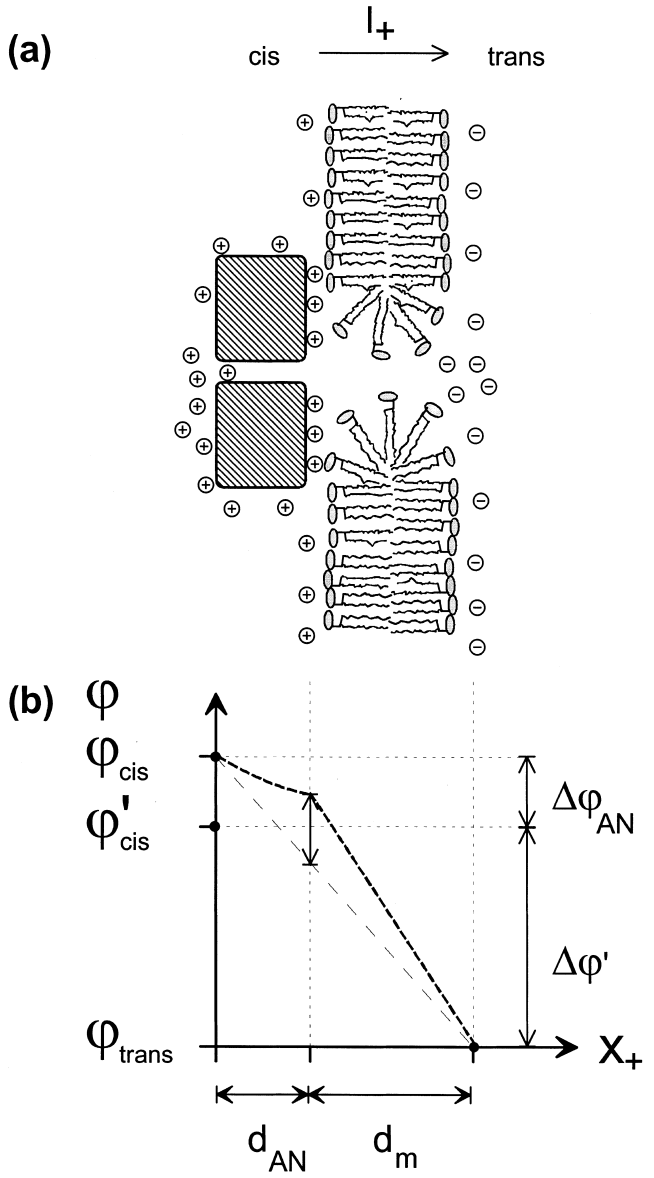

Fig. 12. Interfacial polarization of the type (II) complex configuration and the presumed electric potential profile along the X_+-axis. (a) Charge distributions of an externally induced *trans*-membrane voltage U_m in the direction from *cis* to *trans*. (b) The dashed line represents the potential profile across the protein-membrane complex for $U_{ext} \approx 0.1$ V and $U_{AN} \approx 0.02 \pm 0.005$ V. The nominal potential drops are specified as $\Delta\varphi_{AN} = \Delta\varphi'_{cis} - \varphi_{cis} = -U_{AN}$ and $\Delta\varphi' = \varphi_{trans} - \varphi'_{cis} = -U_{ext}$ [see Eq. (1)], yielding the effective potential drop $\Delta\varphi_m = \varphi_{trans} - \varphi_{cis} = -U_m$ for symmetrical ion concentration conditions.

$$\frac{1}{\tau_o} = \left(\frac{1}{\tau_o}\right)_0 \cdot e^{b^* \cdot U_m^2} \tag{41}$$

is consistent with $K_i(\mathrm{II}) = K_0(\mathrm{II}) \cdot e^{a \cdot U_m^2}$, see Eqs. (29) and (32). For Scheme (8), $K(\mathrm{II}) = k_c/k_{-c}$ and analogous to K we have [33]

$$k = k_0 \cdot e^{b \cdot U_m^2} \tag{42}$$

where the quantity b is related to the electrical

Gibbs activation energy by $G_{act} = RT \cdot b \cdot U_m^2$. Since $K_0(II) = k_c^0/k_{-c}^0$ we readily see that a_i, related to K_i is here connected to b by $a_i = b_c^i - b_{-c}^i$. For membrane voltages $|U_m| \leq 0.1$ V, where $K(II) \leq 0.05$, we may use the approximation $1/\bar{\tau}_o = k_{-c}[1 + K(II)] = k_{-c}$. Therefore $b_{-c} = b^* = 113.9\ V^{-2}$ and $b_c = a_i + b_{-c} = 163.9\ V^{-2}$.

Analogous to r_p and α_i related to a_i, we readily can calculate the activation polarizabilities α_c^i and α_{-c}^i by applying Eq. (36).

Of course, the value $\bar{\tau}_o = 2.13$ s at $U_m = 0$ is an extrapolated value for $U_m = 0$. Note that at $U_{ext} = 0$, no electrical measurement is possible at symmetrical salt concentrations.

Remarkably, it is found that for all experimental conditions represented in Fig. 11: symmetrical 0.05 M Ca^{2+}, symmetrical 1.2 M K^+ and also asymmetrical 1.2 M K^+ (*cis*)/0.014 M K^+ (*trans*), the data can be satisfactorily fitted with one and the same a_i and $f_i^o(II)$ value, respectively. Hence $a = 50\ V^{-2}$ and $f^o(II) = 0.03$ are characteristic quantities of the combined annexin V-bilayer channel complex, independent of the ion type. At $U_m = 0$, we have $U_{ext} = -U_{AN} = -0.02$ V. Under symmetrical concentration conditions, $K_0(II) = f^o(II) = 0.03$ formally means a 3% contribution of, for example $g_{Ca}^o = 69$ pS to $g_{Ca}(II)$. At $U_m = 0.1$ V, $K(II)$ increases up to 0.05 and $f(II) = 0.048$. At $U_m = 0.2$ V, $K(II)$ increases up to 0.22 and $f(II) = 0.22$. It appears that here the entire protein (Ca^{2+})–lipid complex represents the voltage-dependent gating system. Both the multipolar protein conformation and the strong coupling to the field-induced electric pore formation in the lipid phase immediately under the pore are reflected in the characteristic, quadratic voltage dependence, yielding the overall electric polarizability parameter as a measure for the gating flexibility and charge displaceability.

If $g_i(II)$ would be a functional of $e^{a \cdot U_m}$, i.e. the voltage-dependence of the Gibbs gating reaction energy is linear, the symmetrical charge displacement of the multipolar system is equivalent to a symmetrical rotatory alignment of permanent dipoles relative to the membrane normal. Such dipole alignment can be asymmetrical with respect to positive and negative voltages as in the case of rectifiers, for instance, the Clavibacter anion channel protein [34].

In any case, if protein gating of ion flows is observed, the assumption of multipolar fixed charge displacements is more realistic than the assumption of a free gating charge being moved across a part of the membrane thickness [27]. Symmetries become only apparent, if we include into the voltage dependence U_m: potential contributions of screened fixed surface charges by the lipid phase as well as by the protein, either adsorbed and occluding bridging ions or as a membrane-spanning protein configuration. Annexin V is a beautiful example where both cases are realized.

Acknowledgements

We thank the Deutsche Forschungsgemeinschaft for grant Ne 227/9-3 to E.N.

Appendix A

The fraction f_2 of double trimers T_2 (hexamer) for the dimerization reaction

$$T_2 \rightleftharpoons 2\,T \tag{A1}$$

where the equilibrium constant is $K_2 = [T]^2/[T_2]$.

The fraction of hexamers is defined as

$$f_2 = \frac{2[T_2]}{T_t} = \frac{2[T_2]}{2[T_2] + [T]} = \frac{[T]}{[T] + K_2/2} \tag{A2}$$

where, according to mass conservation, the total trimer concentration is $[T_t] = [T] + 2[T_2]$.

Substitution and rearrangements yield:

$$[T] = \frac{1}{4}\left\{\sqrt{K_2(K_2 + 8[T_t])} - K_2\right\} \quad \text{(A3)}$$

Substitution in Eq. (A2) gives:

$$f_2 = \frac{\sqrt{K_2(K_2 + 8[T_t])} - K_2}{\sqrt{K_2(K_2 + 8[T_t])} + K_2} \quad \text{(A4)}$$

where the dependence on the total trimer concentration $[T_t] = 3[\mathrm{AN}_t]$ is readily expressed in terms of the total annexin V concentration $[\mathrm{AN}_t]$.

The trimer reaction is coupled to two other equilibria: the surface adsorption of the annexin V (AN) monomers according to

$$\mathrm{AN} \rightleftharpoons \mathrm{AN}_b \quad \text{(A5)}$$

and the trimerization of AN_b according to

$$3\,\mathrm{AN}_b \rightleftharpoons T_b \rightleftharpoons T. \quad \text{(A6)}$$

In electric fields these reactions are shifted from the surface-bound trimer T_b to the membrane-spanning configuration T (see Fig. 10).

For simplicity we lump the separate reactions together into the overall process

$$3\mathrm{AN} \rightleftharpoons T \quad \text{(A7)}$$

with the overall constant $K_T = [\mathrm{AN}]^3/[T]$ and substitute $[T] = K_T^{-1}\cdot[\mathrm{AN}]^3$ into Eq. (A2).

We obtain

$$f_2 = \frac{[\mathrm{AN}]^3}{[\mathrm{AN}]^3 + \bar{K}^3} \quad \text{(A8)}$$

where $\bar{K} = [(K_2/2)\cdot K_T]^{1/3}$. Eq. (A8) is the basis of the interpretation of Fig. 5, where the exponent 3 in $[\mathrm{AN}]^3$ matches the Hill coefficient $h \approx 3$.

Since the amount of protein associated with the bilayer membrane is extremely small compared with the content of the protein in the bath solution, we also may readily use the approximation $[\mathrm{AN}] = [\mathrm{AN}_t]$ in Eq. (A8).

References

[1] B.A Seaton, Annexins: Molecular Structure To Cellular Function, Springer Verlag, Heidelberg, 1996.

[2] R. Huber, J. Römisch, E.-P. Paques, The crystal and molecular structure of human annexin V, an anticoagulant protein that binds to calcium and membranes, EMBO J. 9 (1990) 3867–3874.

[3] R. Huber, M. Schneider, I. Mayr, J. Römisch, E.-P. Paques, The calcium binding sites in human annexin V by crystal structure analysis at 2.0 A resolution. Implications for membrane binding and calcium channel activity, FEBS Lett. 275 (1990) 15–21.

[4] R. Huber, R. Berendes, A. Burger, M. Schneider, A. Karshikov, H. Luecke, Crystal and molecular structure of human annexin V after refinement. Implications for structure, membrane binding and ion channel formation of the annexin family of proteins, J. Mol. Biol. 223 (1992) 683–704.

[5] R. Berendes, D. Voges, P. Demange, R. Huber, A. Burger, Structure-function analysis of the ion channel selectivity filter in human annexin V, Science 262 (1993) 427–430.

[6] P. Demange, D. Voges, J. Benz et al., Annexin V: the key to understanding ion selectivity and voltage regulation? TIBS 19 (1994) 272–276.

[7] A. Burger, D. Voges, P. Demange, C.R. Perez, R. Huber, R. Berendes, Structural and electrophysiological analysis of annexin V mutants. Mutagenesis of human annexin V, an in vitro voltage-gated calcium channel, provides information about the structural features of the ion pathway, the voltage sensor and the ion selectivity filter, J. Mol. Biol. 237 (1994) 479–499.

[8] S. Liemann, J. Benz, A. Burger et al., Structural and functional characterization of the voltage sensor in the ion channel human annexin V, J. Mol. Biol. 258 (1996) 555–561.

[9] D. Voges, R. Berendes, P. Demange et al., Structure and function of the ion channel model system annexin V, Adv. Enzymol. Relat. Areas Mol. Biol. 71 (1996) 209–239.

[10] P. Läuger, Ionic channels with conformational substates, Biophys. J. 47 (1985) 581–591.

[11] H.A.M. Andree, C.P.M. Reutelingsperger, R. Hauptmann, H.C. Hemker, W.T. Hermens, G.M. Willems, Binding of vascular anticoagulant a (VACα) to planar phospholipid bilayers, J. Biol. Chem. 265 (1990) 4923–4928.

[12] C. Pigault, A. Follenius-Wund, M. Schmutz, J.-M. Freyssinet, A. Brisson, Formation of two-dimensional arrays of annexin V on phosphatidylserine-containing liposomes, J. Mol. Biol. 236 (1994) 199–208.

[13] N.O. Concha, J.F. Head, M.A. Kaetzel, J.R. Dedman, B.A. Seaton, Annexin V forms calcium-dependent trimeric units on phospholipid vesicles, FEBS Lett. 314 (1992) 159–162.

[14] G. Mosser, C. Ravanat, J.-M. Freyssinet, A. Brisson,

Sub-domain structure of lipid-bound annexin-V resolved by electron image analysis, J. Mol. Biol. 217 (1991) 241–245.
[15] D. Voges, R. Berendes, A. Burger, P. Demange, W. Baumeister, R. Huber, Three-dimensional structure of membrane-bound annexin V. A correlative electron microscopy X-ray crystallography study, J. Mol. Biol. 238 (1994) 199–213.
[16] K. Toensing, S. Kakorin, E. Neumann, S. Liemann, R. Huber, Annexin V and vesicle membrane electroporation, Eur. Biophys. J. 26 (1997) 307–318.
[17] A. Burger, R. Berendes, D. Voges, R. Huber, P. Demange, A rapid and efficient purification method for recombinant annexin V for biophysical studies, FEBS Lett. 329 (1993) 25–28.
[18] T. Funakoshi, R.L. Heimark, L.E. Hendrickson, B.A. McMullen, K. Fujikawa, Human placental anticoagulant protein: isolation and characterization, Biochemistry 26 (1987) 5572–5578.
[19] P.K. Smith, R.I. Krohn, G.T. Hermanson et al., Measurement of protein using bicinchoninic acid, Anal. Biochem. 150 (1985) 76–85.
[20] M. Montal, P. Mueller, Formation of bimolecular membranes from lipid monolayers and a study of their electrical properties, Proc. Natl. Acad. Sci. USA 12 (1972) 3561–3566.
[21] D. Voges, 3-D-Struktur des membrangebundenen Annexin V mittels Elektronenmikroskopie, Praeparation und Charakterisierung von Annexin VI, Simulation der Annexin V Modulbewegung, Modell der Dielektrizitaetskonstante in Proteinen, PhD thesis, Technische Universitaet Muenchen, 1995.
[22] E. Neumann, S. Kakorin, K. Toensing, Fundamentals of electroporative delivery of drugs and genes, Bioelectrochem. Bioenerg. 48 (1999) 3–16.
[23] H. Luecke, B.T. Chang, W.S. Maillard, D.D. Schlaepfer, H.T. Haigler, Crystal structure of the annexin XII hexamer and implications for bilayer insertion, Nature 378 (1995) 512–515.
[24] P.W. Atkins, Physical Chemistry, Oxford University Press, Oxford, 1998.
[25] M. Eigen, L. DeMaeyer, Relaxation methods, in: S.L. Fries et al. (Ed.), Techniques of Organic Chemistry, vol. 8, 2nd ed, New York, Wiley, 1963, pp. 495–1054.
[26] A.L. Hodgkin, B. Katz, The effect of sodium ions on the electrical activity of the giant axon of the squid, J. Physiol. 108 (1949) 37–77.
[27] B. Hille, Ionic Channels of Excitable Membranes, Sinauer Associates Inc, Sunderland, MA, 1992.
[28] E. Neumann, E. Boldt, Membrane electroporation: biophysical and biotechnical aspects, in: M.J. Allen, S.F. Cleary, F.M. Hawkridge (Eds.), Charge and Field Effects in Biosystems-2, Plenum Press, New York, 1989, pp. 373–382.
[29] E. Neumann, Membrane electroporation and direct gene transfer, Bioelectrochem. Bioenerg. 28 (1992) 247–267.
[30] S. Kakorin, S.P. Stoylov, E. Neumann, Electro-optics of membrane electroporation in diphenylhexatriene-doped lipid bilayer vesicles, Biophys. Chem. 58 (1996) 109–116.
[31] E. Neumann, The relaxation hysteresis of membrane electroporation, in: E. Neumann, A.E. Sowers, C. Jordan (Eds.), Electroporation and Electrofusion in Cell Biology, Plenum Press, New York, 1989, pp. 61–82.
[32] E. Neumann, S. Kakorin, Electroporation of curved lipid membranes in ionic strength gradients, Biophys. Chem. 84 (2000) in press.
[33] E. Neumann, Chemical electric field effects in biological macromolecules, Prog. Biophys. Mol. Biol. 47 (1986) 197–231.
[34] T. Schuerholz, L. Dloczik, E. Neumann, Single-channel analysis of the anion channel-forming protein from the plant pathogenic bacterium *Clavibacter michiganense* ssp. *nebraskense*, Biophys. J. 64 (1993) 58–67.